

Peen forming and stress peen forming of 2024–T3 aluminum sheets. Part 1: 3D scans and residual stress measurements

Pierre A. Fauchoux, Hong Yan Miao, Martin Levesque, Frédérick P. Gosselin

*Laboratory for multiscale mechanics (LM2), Département de Génie Mécanique,
Polytechnique Montréal, Montréal, QC, Canada*

Abstract

Aluminum skins on the lower wings of most commercial aircraft are shaped using shot peen forming. This process, which involves bombarding the skins with hard shot, uses nonuniform plastic flow to induce curvatures—in the same way that differential expansion makes metal bilayers bend when heated. Here, we investigate experimentally how constraining conditions affect the final shape of peen formed parts. We report peen forming experiments for 4.9 mm thick rectangular 2024–T3 aluminum sheets of different aspect ratios uniformly shot peened on one face with a low intensity saturation treatment. Some specimens were free to deform during peening while others were elastically prestressed in a four-point bending jig. For each aspect ratio and prestress condition, residual stresses were measured near the peened surface with the hole drilling method. Additional residual stress profiles were also obtained with the slitting method. The residual stress measurements show that the progressive deformation of unconstrained specimens had the same effect as an externally applied prestress. For the peening conditions investigated, this progressive deformation caused unconstrained strips to exhibit curvatures 33 % larger than identical strips held flat during peening. Furthermore, we found that the relative importance of material anisotropy and geometric

*Corresponding author

Email address: frederick.gosselin@polymtl.ca (Frédérick P. Gosselin)

URL: <http://www.polymtl.ca/lm2> (Frédérick P. Gosselin)

effects did determine the bending direction of unconstrained specimens.

Keywords: Shot peening, peen forming, metal forming, residual stress, initial stress, distortion, 2024–T3 aluminum

1. Introduction

Shot peen forming stands out among sheet metal forming processes by its flexibility and low operating costs. The process consists in bombarding thin metal parts with hard shot such that the incompatibility of deformations
5 between the plastically deformed surface layers and the underlying material causes the part to bend, as illustrated schematically in Figure 1a. Typical applications include forming large wing-skin panels for commercial aircraft (Baughman, 1970; Levers, 2010), forming doubly curved panels for space launchers (Hornauer and Köhler, 1990; Merino et al., 2017), and correcting
10 small out-of-tolerance distortions on machined parts (Skinner, 1978; Eckersley and Axline, 1991).

Because peening stretches the material in all directions, uniformly peened parts tend to deform into spherical shapes, as illustrated in Figure 1a. To break this symmetry, process engineers use a technique called stress peen
15 forming where jigs are used to hold parts into a bent shape during peening. This results in larger curvatures in the bending direction and smaller curvatures in the transverse direction, as illustrated in Figure 1b. The final curvatures of stress peen formed parts was repeatedly observed to be proportional to the prestress curvature. Table 1 compiles the publicly available
20 results we found on stress peen forming of uniformly peened rectangular plates.

While many experimental studies dedicated to shot peening investigated residual stresses, roughness, and changes in microstructure induced by peening treatments, see for example the the literature reviews of (Gariépy, 2012),
25 comparatively fewer considered peening induced distortions. Among these, most aimed at generating data to establish process parameters for a given application. For example, Kulkarni et al. (1981) investigated the influence of shot size, shot velocity, and the plate’s aspect ratio on the curvature of 610 mm long 2024 and 7050 rectangular aluminum sheets that were free to
30 deform during peening; Villalva-Braga (2011) generated a dataset of curvature and residual stress profiles for 400×50 mm 7050 and 7475 aluminum

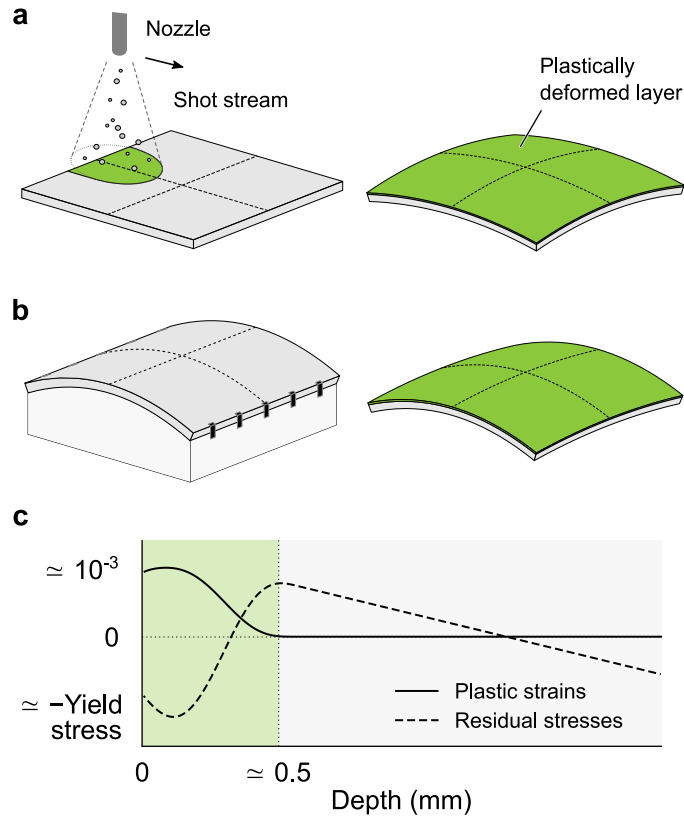


Figure 1. Peen forming of a metal plate. Repeated impacts plastically deform a thin layer of material which, as it stretches, causes the plate to deform. (a) Plates peened with low intensity treatments, thick plates, and plates with high aspect ratios tend to deform into spherical shapes. (b) Prebending a plate during peening results in larger curvatures in the prestress direction and smaller curvatures in the transverse direction. (c) Typical in-plane plastic strain and residual stress profiles after uniform peening. The in-plane expansion of the upper layers is resisted by the bulk, which causes compressive residual stresses near the surface. Conversely, the upper layers stretch the bulk, which causes tensile stresses deeper into the material. In the bulk, stresses vary linearly owing to the stretching and bending of the specimen.

strips for various prestress conditions; and Miao et al. (2010) reported similar results for 76×19 and 76×76 mm 2024–T3 aluminum strips. Additional references featuring conventional and stress peen forming experimental results are listed in Tables 1 and 2.

Of these studies, only half report curvature measurements in more than one direction, and only three report residual stress measurements in more than one direction. However, several phenomena are expected to cause anisotropic curvatures and residual stresses. These include the known plastic anisotropy of rolled aluminum sheets used for most experiments (Prime, 2017), anisotropic initial residual stresses inherited from the manufacturing process of the sheets (e.g., quenching or rolling), and prestress, whether externally applied with a jig (Figure. 1b) or resulting from the progressive deformation of an unconstrained part (Figure. 1a). Although these phenomena were suspected to account for most of the discrepancies between experiments and numerical simulations of the process previously reported by our team in Gariépy et al. (2013) and Faucheux et al. (2018), this intuition could not be confirmed at the time due to a lack of experimental data.

In this paper, we investigate experimentally the effect of material anisotropy and prestress on the final deformed shape of uniformly peened aluminum sheets. The paper is structured as follows. Section 2 presents the materials and methods. Section 3 summarizes the results of (i) conventional peen forming experiments conducted on 4.9 mm thick and 1016 mm long 2024–T3 aluminum alloy rectangular sheets of different aspect ratios and (ii) stress peen forming experiments conducted on 508×127 mm strips of the same alloy. These tests probed the influence of the alignment of the specimens with respect to the rolling direction, that of their aspect ratio, and, to a lesser extent, that of the peening trajectory on curvatures and residual stresses. Finally, Section 4 presents a preliminary, qualitative, analysis of the results. A detailed analysis of the results is presented as a companion paper (Part 2).

2. Materials and methods

Material. All experiments were conducted on 4.9 mm thick Kaiser Stretched aluminum alloy 2024–T3 sheets purchased from Kaiser Aluminum. The manufacturing process of the sheets included a stress relief by a stretching step. Metallographic specimens etched with Keller’s reagent revealed large elongated grains of mean aspect ratio 7.1:3.6:1.0 along the longitudinal (L),

Table 1
 Compilation of publicly available papers and reports featuring stress peen forming experimental results for uniformly peened rectangular plates. Not included are several conference papers that were not readily available, and papers written in languages that none of the authors were familiar with. This includes some possibly highly relevant studies in the German, Chinese, and Japanese-speaking literature. Brackets indicate ranges.

Reference	Material	Dimensions		Peening treatment ^a		Increment in curvature per unit increment in prestress curvature		Reported results		Notes		
		Length (mm)	Width (mm)	Thickness (mm)	Media ^b	Coverage ^c (%)	Intensity ^d ($\times 10^{12}$ in)	Prestress radius of curvature (mm)	Along prestress direction (-)		Along transverse direction (-)	Deformed shape
Barent and Toth (1984)	7075-T7053 Al	792	508	17.3	Saturation: 0.6 mm steel Forming: 3.2 mm steel	Saturation: 100 Forming: between 60 and 80	-	1700 (along short side)	-	-	Curvature along both directions; Same 3D scans	Profiles, some in both directions (XRD)
Hu et al. (2015)	2024-T351 Al	67	67	4	Laser peening	-	-	∞ , 2000, 1000, 667	0.41	0.14	Curvature along both directions	Surface stress (XRD)
Li (1981)	LY12CZ Al	76	76	2	[2, 2.5] mm iron	100	-	∞ , 5000, 1000, 500, 250	0.60/ ^f	-0.06/ ^f	Arc height	-
Miao et al. (2010)	2024-T3 Al	76	19	1.6	Z425	100	5, 7.4, 8.7 A	∞ , 720, 360, 240	[0.41, 0.65]	-	Arc height (in both directions for square specimens); some line scans	Profiles along prestress direction (XRD)
Miao et al. (2011)	7075-T7053 Al	76	76	1.6	Z425	100	5, 7.4, 8.7 A	∞ , 720, 360, 240	[0.40, 0.65]	[-0.08, -0.17]	-	Profiles along prestress direction (layer removal)
Skinner (1978)	7075-T7053 Al	305	44	6.35	Saturation: S230 Forming: 3/16" ball bearings	Saturation: 100 Forming: 20, 40, 60, 80	Saturation: 6 A Forming: 10, 12, 15 C	∞ , 1050, 825, 625	-	-	Curvature along prestress direction	Profiles along prestress direction (XRD)
Villalba-Bejar (2011)	7050-T7451 Al	400	50	2, 5, 10, 15	S230, S550, 1/8"	From 60 to 200	-	1270, 850, 420, 170 ^g	-	-	Curvature along prestress direction	Profiles along prestress direction (XRD)
Wang et al. (2014)	7150 Al	300	200	8, 10, 12	3.18 mm	From \leq 50 to 100	-	810, 680, 540	-	-	Curvature along prestress direction	-
Xiao et al. (2016)	2024-T351 Al	100	30	5	Brinell indenter (3.175 mm diam.) 3.175 mm steel	Variable	-	∞ , 1252, 626	[0.27, 0.46] ^h	[-0.21, -0.12] ^h	Curvature along both directions	-
Zhang et al. (2019)	2024-T351 Al	120	50	1.5, 2.0, 3.0, 3.5	Ultrasonic peening (indenter 3 mm in diam.)	22, 35, 46	-	∞ , 1200, 1000, 800, 600, 400	0.63 ⁱ 0.18 ^j 0.33 ^k 0.33 ^l	-0.05 ⁱ -0.05 ^j -0.08 ^k -0.07 ^l	Curvature along both directions	-
This study	2024-T3 Al	508	127	4.9	SCCV28	100	12 A	∞ , 370, 1901, 1265, 652	[0.22, 0.23]	[-0.03, -0.13]	Curvature along both directions	Profiles in both directions (hole drilling)

^a Process parameters such as air pressure, mass flow, and exposure time are usually available when intensity or coverage are not reported.

^b Conventional designation or diameter.

^c As defined in SAE standard J2277 (2013), unless otherwise specified.

^d NPD # used for X-ray diffraction.

^e Estimated from figure 1 of Li (1981). The curve deviate from linearity for prestress radii of curvature larger than 4000 mm.

^f Estimated from figure 21 of Xiao et al. (2016), where h is the thickness of the plate, E is Young's modulus, and σ is 90 % of the yield stress.

^g Estimated from figure 11 of Zhang et al. (2019).

^h Results are reported in mm.

ⁱ Results are reported in mm.

^j Results are reported in mm.

^k Results are reported in mm.

^l Results are reported in mm.

^m Half the specimens was cut with the long side aligned with the rolling direction while the other half was cut with the long side aligned with the transverse direction.

Table 2
 Compilation of publicly available papers and reports featuring shot peen forming experimental results for uniformly peened rectangular plates. Not included are several conference papers that were not readily available, and papers written in languages that none of the authors were familiar with. This includes some possibly highly relevant studies in the German, Chinese, and Japanese-speaking literature.

Reference	Material	Dimensions			Peening treatment ^a			Reported results			
		Length (mm)	Width (mm)	Thickness (mm)	Media ^b	Coverage ^c (%)	Intensity ^d ($\times 10^{-3}$ in)	Shot speed (m/s)	Specimens constrained during peening	Deformed shape	Residual stress ^e
Chao et al. (1995)	SAE 1070 steel	75	19	1.29	Similar to S110	Variable	8 A	45	Yes	Curvature in both directions; one line scan	Profiles in both directions (XRD)
Chiu et al. (1990)	2024-T62 Al. 7075-T76 Al.	360	130	4.5 4.0	From S230 to S280	100	7 A, 5 C	-	No	Deflection; one line scan	-
Fauchoux et al. (2018)	2024-T3(51) Al.	1000	1000	5, 10, 15	S230 1/8" steel	100	16.8 A	-	No	Curvature in both directions; some line scans	Profiles on thick blocks in one direction (XRD)
Garfepy et al. (2013)	2024-T3 Al.	200	50	10	S230 1/8" steel	100	16.8 A 22.9 C	-	Yes	Arc height; curvature in both directions	Initial stress profiles in both directions (XRD)
Gedineau (2018) ^f	Inconel 718	75	19	5.0, 2.0	S130	125 200	5.1 A 9.1 A	≈ 42	Yes	3D scans, some line scans	Profiles in both directions (XRD)
Johnson et al. (1981)	HE 30 Al., mild steel, pure copper	76	25	3.2	S170, S240	Variable	-	-	Yes	Arc height	-
Kulkarni et al. (1984)	2024-T3(51) and 7050-T6(51) Al.	610	152, 305, 610 ^g	1.6, 4.6, 12.7	0.6 mm steel 1.0 and 1.7 mm steel	Variable	8, 10, 16 A	32, 53, 78	No	Curvature in both directions	Typical values (XRD)
Miao et al. (2010), Garfepy et al. (2011)	2024-T3 Al.	76	19, 76	1.6	Z425	Variable	5 A 7.4 A 8.7 A	35 54 66	Yes	Arc height; curvature in both directions for square specimens	Through thickness profiles on specimens and thick blocks along one direction (XRD)
Vilalva-Braga (2011)	7050-T7451 and 7475-T7451 Al.	400	50	5	S230 S550 S550	Variable	-	16, 22, 29 16, 22, 29 13, 17, 19	Some specimens	Curvature along long side	Profiles along one direction for some 7050 Al. specimens (XRD)
Present study	2024-T3 Al.	1016	254, 508, 1016	4.9	SCCW28	100	12 A	41	No	3D scans	Profiles in both directions (hole drilling, slitting)

^a Process parameters such as air pressure, mass flow, and exposure time are usually available when intensity or coverage are not available.

^b Conventional designation or diameter.

^c As defined in SAE standard J2277 (2013), unless otherwise specified.

^d Almen intensity, as defined in SAE standard J443 (2010), unless otherwise specified.

^e XRD stands for X-ray diffraction.

^f Also reported are microstructural characterization (including EBSD maps), some initial stress profiles, FWHM of XRD measurements, microhardness measurements, and experiments on specimens of complex geometries.

^g Limited results for specimens of other aspects ratio are available in figure 11 of Kulkarni et al. (1981).

Table 3

Mean static properties of the 4.9 mm thick aluminum alloy 2024–T3 sheets tested in this work. These values were averaged over three tests.

Angle w.r. to rolling direction (°)	Young’s modulus (GPa)	Yield stress at 0.2 % (MPa)	Ultimate tensile stress (MPa)	Elongation at fracture (mm/mm)
0	71.5 ± 1.6	381 ± 0	486 ± 1	0.1836 ± 0.0070
45	71.6 ± 3.0	349 ± 1	485 ± 0	0.1920 ± 0.0145
90	71.7 ± 1.5	339 ± 1	489 ± 0	0.1946 ± 0.0058

Mean \pm 95 % confidence interval

long transverse (T), and short transverse (S) directions, respectively. Grains had an average length of 0.268 mm. The largest observed grain length was of 4.7 mm. Static properties were obtained from tensile tests performed at 0°, 45°, and 90° from the rolling direction, as per [ASTM standard B557M-15 \(2015\)](#). Three specimens in each direction were removed from the same sheet (the consistency of properties from one sheet to the next was not assessed). Table 3 lists the measured static properties for each direction. The observed elastic isotropy and mild plastic anisotropy are consistent with other experimental data from the literature ([Bron and Besson, 2004](#); [Seidt and Gilat, 2013](#)).

Peening setup. All specimens were shot peened in the Canablast compressed-air cabinet shown in Figure 2a. The peening cell was equipped with a 6-axis robotic arm for an accurate positioning of the nozzle (M-20iA supplied by Fanuc), with a particle velocity sensor to measure the average shot velocity (Shotmeter G3 supplied by Progressive Technologies), and with a GoPro digital camera to record the peening process application. Shot were recycled. Torn and broken shot were removed by separator screens.

For conventional peen forming experiments, the frame shown in Figure 2c provided a level working surface and stops guaranteed consistent positioning from one specimen to the next. The specimens were otherwise free to deform during peening.

For stress peen forming experiments, specimens were prestressed in the four-point bending jig shown in Figure 2b. The spacing between the 4 support beams could be adjusted and several pairs of beams of different heights were

used to obtain prestress curvatures ranging from 0 to $10.5 \times 10^{-4} \text{ mm}^{-1}$ (or, equivalently, radii of curvatures ranging from infinity to 952 mm).

Peening treatment. High hardness spherically conditioned cut wire steel shot SCCW28 compliant with [AMS standard 2431/8B \(2007\)](#) were used for all treatments. The manufacturer’s specification stated a 55–62 HRC hardness and a nominal diameter of 0.71 mm.

The same treatment, representative of low intensity saturation treatments used in the industry, was applied to all specimens. The nominal peening parameters were a 12A (0.30 mmA) Almen intensity and 100% coverage,¹ which were obtained with the process parameters listed in Table 4. All peen forming experiments were conducted as per [SAE standard J2277 \(2013\)](#); [SAE standard J443 \(2010\)](#); [AMS standard 2430 rev. T \(2015\)](#). Almen tests ran at the five locations indicated by downward pointing triangles in Figure 2c yielded intensities ranging from 11.6 A(0.26 mmA) to 12.0 A(0.30 mmA), which substantiates that intensity was uniform over the working surface. Consistency of the process was ensured by performing additional Almen tests at the center of the specimens at the beginning and at the end of each peening day, or after having peened two plates, whichever was the shortest.

Distribution of impacts after one peening stroke. The distribution of impacts after one peening stroke was characterized by peening a 508×203 mm dummy specimen, the same 2024–T3 aluminum as the test specimens, with the nozzle moving at 22.5 cm/s. At that speed, the density of impacts was low and there was little overlap between dimples. High resolution pictures of the peened surface were taken as the specimen was lit with softened raking lights. The pictures were then stitched together, binarized, and partitioned into bins

¹Alongside shot specifications, Almen intensity and coverage are the two parameters used to characterize peening treatments in the industry. Coverage is the fraction of a surface covered by dents. Intensity is primarily intended as a process control parameter. It is obtained by (i) peening normalized SAE–1070 spring steel strips mounted on a holding fixture in the same conditions as production parts for increasing amounts of time, (ii) measuring their deflection in a standardized Almen gage, and (iii) plotting the deflection as a function of peening time. From these curves, intensity is defined as the value of the deflection which increases by 10% when the peening time is doubled ([SAE standard J443, 2010](#)).

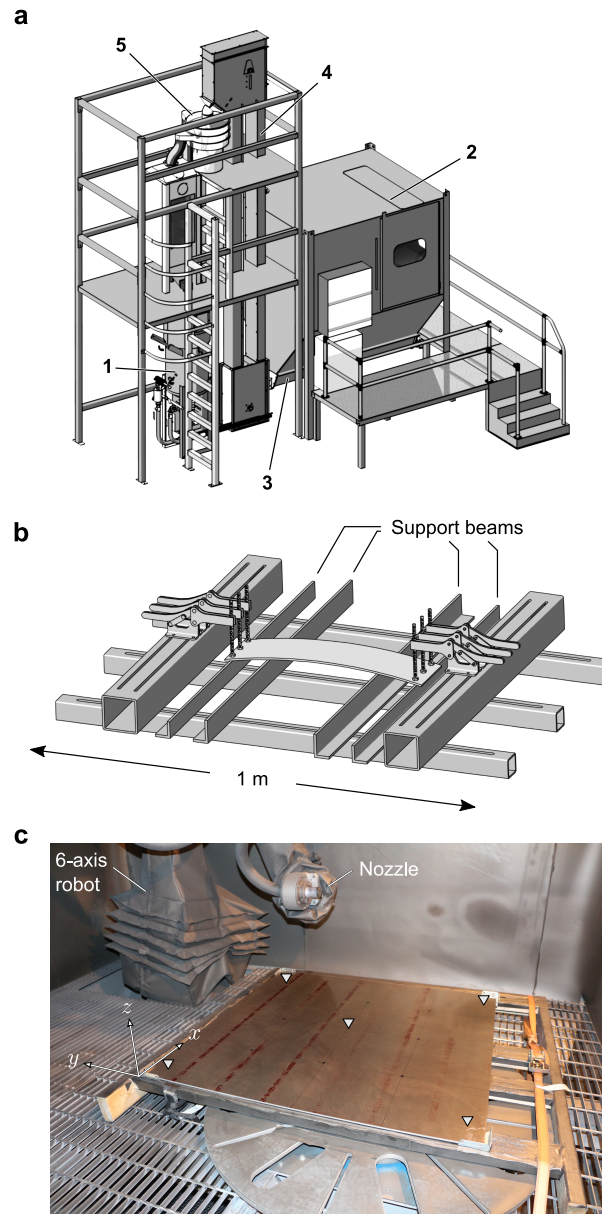


Figure 2. Shot peening setup. (a) Compressed air peening cabinet used for peen forming experiments. Shot are propelled from a pressurized tank (1) into a closed cabinet (2) where they strike the parts. Used shot are collected at the bottom of the cabinet by an endless screw (3) followed by an elevator bucket (4). They are dropped onto a stack of separator screens (5) that removes broken shot before recycling them into the tank. (b) Four-point bending jig used for stress peen forming experiments. The spacing between the 4 support beams could be adjusted. Several pairs of beams of different heights were used to obtain curvatures ranging from 0 to $10.5 \times 10^{-4} \text{ mm}^{-1}$ (associated radii of curvature: from infinity to 952 mm). (c) Interior of the peening cabinet showing the robotic arm and an unpeened $1016 \times 1016 \text{ mm}$ sheet resting on a leveled frame. During conventional peen forming experiments, the sheets were free to deform. Downward pointing triangles show the locations at which Almen intensity was measured.

Table 4

Peening parameters used to obtain a 12×10^{-3} inches A Almen intensity and 100 % coverage with SCCW28 shot.

Nozzle diameter (mm)	Air pressure (Bars)	Mass flow (kg/s)	Shot speed [†] (m/s)	Stand-off distance (cm)	Offset between strokes (mm)	Peening speed (cm/s)	Number of cycles
12.7	1.72	0.12	41	41	67	15	12

[†] Average speed at the exit of the nozzle.

parallel to the peening direction as shown in Figure 3a–b. The distribution of impacts was subsequently estimated by counting the fraction of white pixels in each bin. Note that, although the shape of white spots on binarized images was markedly different from that of the dimples, their location was correct and it was assumed that variations in shape from one spot to the next were compensated by the many impacts considered. Figure 3c shows the distribution of white pixels as well as a least-squares fit of the data with equation

$$f(x) = A \left(1 - 4 \left(\frac{x}{w} \right)^2 \right)^{\beta-1},$$

110 where $A = 4.78$ is the amplitude in % of white pixels, $w = 205$ mm is the width, and $\beta = 6.32$ is a dimensionless adjustable parameter. Superimposing several of these distributions allows to estimate the uniformity of the number of impacts per unit surface after several parallel overlapping strokes, as shown in Figure 3d. In this case, we found that the largest spacing between parallel
115 strokes that yielded variations smaller than 1 % in the number of impacts per unit surface was 67 mm.

Peening trajectories. All specimens were peened with a succession of parallel strokes, as shown in Figure 4. To ensure that the nozzle remained approximately normal to the peened surface as specimens deformed, the treatment was broken into 12 cycles and the trajectory for cycle $n + 1$ was computed based on the shape of the specimen at the end of cycle n . The latter was estimated by recording the position of target points drawn on the peened surface with a stylus mounted on the head of the 6-axis robot and by fitting a surface of equation

$$z(x, y) = ax^2 + by^2,$$

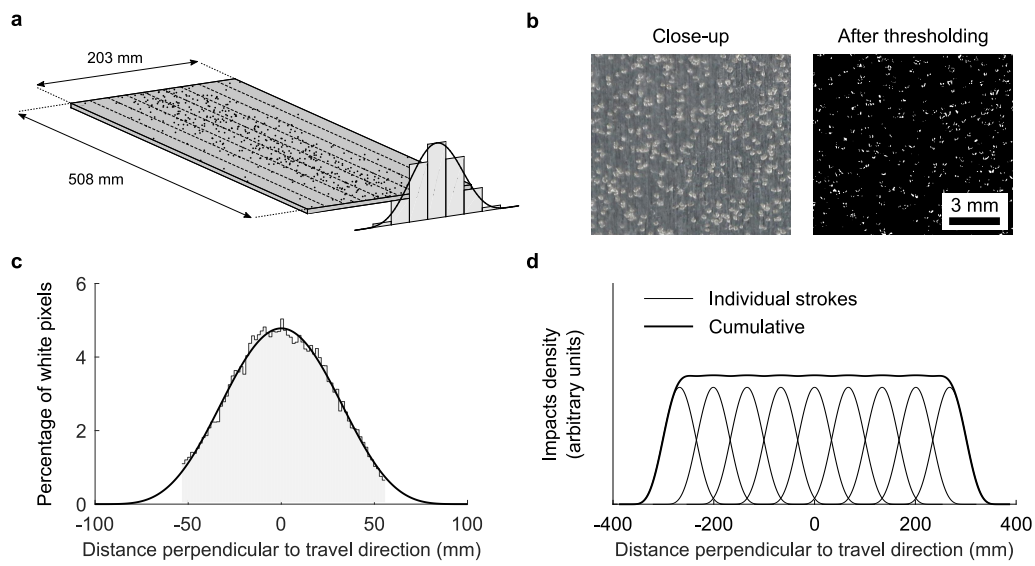


Figure 3. The density of impacts after a single straight peening stroke was characterized by (a) peening a dummy specimen, (b) thresholding high resolution pictures of the peened surface such that dimples appeared as white spots, and (c) counting the fraction of white pixels in bins parallel to the peening stroke. (d) The density of impacts after several parallel overlapping strokes was estimated by superimposing several of these distributions. In (d), the distributions for individual strokes are spaced 67 mm apart.

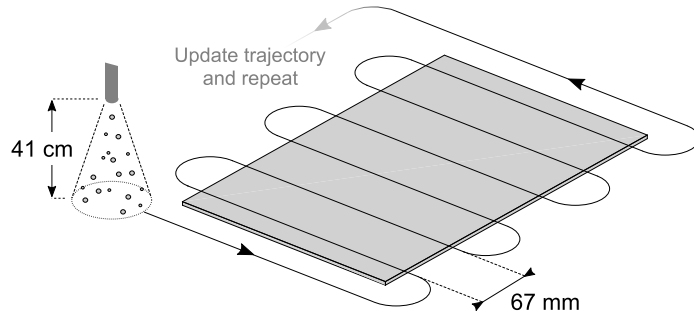


Figure 4. Nozzle trajectory for the first peening cycle. The trajectory was updated at the end of each cycle based on the current shape of the part so that the nozzle remained normal to, and at a constant distance from, the surface. Half of the specimens was peened with strokes parallel to the L direction while the other half was peened with strokes parallel to the T direction.

through these points, where a and b are adjustable parameters and x , y , and z are defined in the place of the flat plate as shown in Figure 2c. To achieve uniform coverage, the offset between two successive strokes was set to 67 mm based on the analysis of the distribution of impacts from the previous paragraph. Visual inspection confirmed that coverage was uniform. The peening speed listed in Table 4 was set so that 100% coverage was reached after 12 peening cycles. Coverage was estimated as per SAE standard J2277 (2013) from magnified pictures of the peened surface.

Specimens. For comparison purposes, specimens similar to those used in Kulkarni et al. (1981) were selected for conventional peen forming experiments. The specimens consisted of 10 rectangular sheets of 4:1, 2:1, 1:1, 1:2, and 1:4 aspect ratio, 1016 mm along the long side. Two sheets were peened per aspect ratio. Half of the specimens were peened with strokes parallel to the L direction while the other half were peened with strokes parallel to the T direction. Table 5 lists the specimens used for conventional peen forming experiments.

Specimens used for stress peen forming experiments were 508×127 mm strips. The prestress curvatures were 0, 2.7, 5.1, 8.3, and $10.5 \times 10^{-4} \text{ mm}^{-1}$. Strips with zero prestress curvature were held flat during peening. These curvatures induce stresses of 0, 47, 90, 146, and 184 MPa on the upper face of the strips, which is well below the yield stress of the material. Two strips with their long side aligned with the L direction and two strips with their long side aligned

Table 5

Specimens used for conventional peen forming experiments.

Specimen ID	Dimensions (mm)		Peening strokes	Residual stress measurements
	Along L	Along T		
Sheet 4:1-L	1016	254		Hole drilling
Sheet 2:1-L	1016	508		-
Sheet 1:1-L	1016	1016	Parallel to L	Hole drilling
Sheet 1:2-L	508	1016		Hole drilling, Slitting
Sheet 1:4-L	254	1016		Hole drilling, (XRD)
Sheet 4:1-T	1016	254		(XRD)
Sheet 2:1-T	1016	508		Hole drilling
Sheet 1:1-T	1016	1016	Parallel to T	(XRD)
Sheet 1:2-T	508	1016		-
Sheet 1:4-T	254	1016		-

with the T direction were peened for each prestress condition, except for the
140 $8.3 \times 10^{-4} \text{ mm}^{-1}$ prestress condition where three strips were used. All strips
were peened with strokes parallel to their long side.

3D scans and curvature measurements. After peening, all sheets used for
conventional peen forming experiments were scanned with a coordinate mea-
suring machine (Mitutoyo, Crysta-Apex 163011) equipped with a REVO®
145 5-axis measurement system. Measurements were taken every 4 mm in con-
tinuous scanning mode along several lines parallel to the long and the short
directions.

Strips used for stress peen forming experiments were scanned along the lines
parallel to the long and short directions passing through the center of the
150 specimens (i) before peening while held in the prestressing jig and (ii) after
peening after all constraints had been released. Measurements while on the
prestressing jig were taken every 25 mm with a stylus mounted on the head
of the 6-axis robot. Measurements after peening were taken every 3 mm with
an electronic indicator (CDI Chicago, Logic ALG, A2720).

155 Coupons used for residual stress measurements (see next paragraph) were
also scanned with an electronic indicator, as just described.

Curvatures were computed as $\kappa = p''/(1 + p'^2)^{3/2}$, where p is an eighth-order

polynomial fit to the 3D scans along the dotted lines shown in Figure 1a and where the prime denotes differentiation with respect to the direction along which the curvature is computed. All curvatures reported in the rest of the article are average curvatures averaged over the central 50% of the scanning lines.

Residual stress measurements. Due to its high sensitivity to low residual stress levels (Prime, 1999), the slitting method was used to characterize initial residual stresses on as-rolled sheets. Hill-Engineering performed the measurements on two 51×51 mm coupons (one coupon for each direction). A single strain gage located opposite to the cut on the back face of the specimens was used. The slot was incrementally cut by wire electric discharge machining by 0.051 mm to 0.254 mm increments over the first 3.43 mm. Residual stresses were computed as described in Schajer and Prime (2006), with unit pulse basis functions, Tikhonov regularization, and compliances computed from 2D plane-strain finite element simulations. The procedure used for uncertainty analysis is detailed in Prime and Hill (2006).

The incremental hole drilling method was used to measure residual stresses in

- 254×254 mm coupons removed from selected specimens used for conventional peen forming experiments (one coupon per aspect ratio; see Table 5);
- 254×127 mm coupons removed from some strips used for stress peen forming experiments (one coupon per prestress condition).

The coupons were removed from the center of the sheets with a lubricated jigsaw (except for sheet 1:4-L for which the coupon was removed from the end). Residual stresses were measured at the center of the coupons, far away from the edges, to minimize the effect of cutting induced plastic deformations and heating on measurement. Hill-Engineering, performed all measurements as per ASTM standard E837-08 (2008). The holes were 2 mm in diameter and were drilled in 0.051 mm increments to a final depth of 1.020 mm. Uncertainty calculations—which are not part of ASTM standard E837-08 (2008)—were similar to those used for slitting measurements.

One additional slitting measurement was performed on sheet 1:2-L to validate the hole drilling measurements. Two 15.24×17.78 mm coupons were

removed by electric discharge machining 2.5 cm away from the edges of the coupon used for hole drilling measurements. Such small coupons were needed to ensure that the depth of the slot was approximately constant as slot cut with straight EDM wires into curved specimens are deeper at the center than they are near the edges, as illustrated in Figure 5. The curvature of the coupons was estimated to $3 \times 10^{-4} \text{ mm}^{-1}$, which gave a variation in the depth of the cut of $\delta \simeq \kappa w^2/8 \simeq 9 \times 10^{-3} \text{ mm}$ when cutting along the short side, where κ and w are defined as in Figure 5b. Such variations were a posteriori confirmed to be much smaller than the characteristic length over which residual stresses varied (see Figures 9 and 10a).

X-ray diffraction measurements were attempted on several specimens (Table 5) but the large grain size and texture of the material prevented obtaining meaningful results.

3. Results

3.1. Conventional peen forming experiments

Figure 6 shows 3D scans of the final deformed shape of sheets used for conventional peen forming experiments and Table 6 lists their curvatures. We see that:

- Sheets of 1:1 aspect ratio deformed into cylinders;
- Sheets of 1:2 and 2:1 aspect ratio assumed distinct nonzero curvature in both directions, with one of the curvatures being approximately one order of magnitude smaller than the other;
- Sheets of 1:4 and 4:1 assumed elliptical shapes, with curvatures in all directions having the same order of magnitude;
- All specimens had their largest curvature along the L direction.
- Identical specimens peened with strokes parallel to either the L or the T direction assumed almost identical shapes, with differences in curvatures of less than 7% between the two sets of sheets;

These results are consistent with those reported by [Kulkarni et al. \(1981\)](#) who observed the same deformed shapes for 4.6 mm thick and 610 mm long 2024-T3 and 7050-T6 aluminum specimens of 4:1, 2:1, 1:1, 1:2, and 1:4 aspect

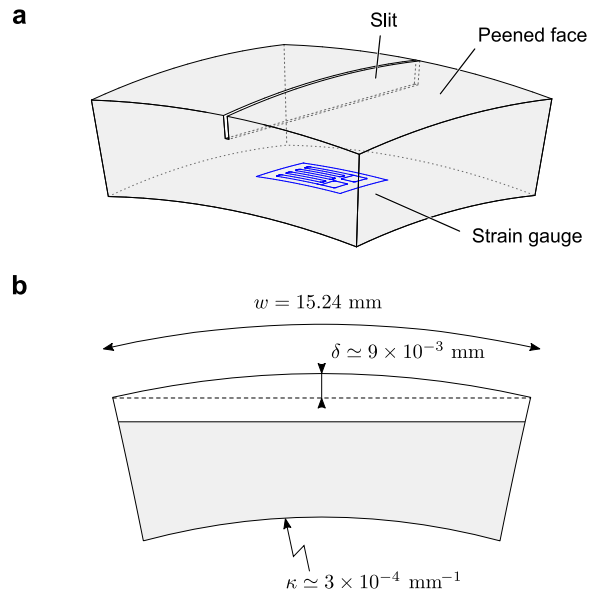


Figure 5. Schematic illustration of the specimens used to measure peening-induced residual stresses with the slitting method (curvature amplified for clarity). (a) Strains were measured with a single strain gauge attached to the back face of the specimens as the latter were cut with a straight EDM wire. (b) Since peened specimens are curved, the slot is deeper near the center than it is near the edges. Because slitting returns stresses averaged over the length of the slot, small $15.24 \times 17.78 \text{ mm}$ coupons were used so that the variation in the depth of the slot, which was estimated to $\delta \simeq 9 \times 10^{-3} \text{ mm}$ from the curvature of the coupons, was small, when compared to the characteristic length over which residual stresses varied (see Figures 9 and 10a).

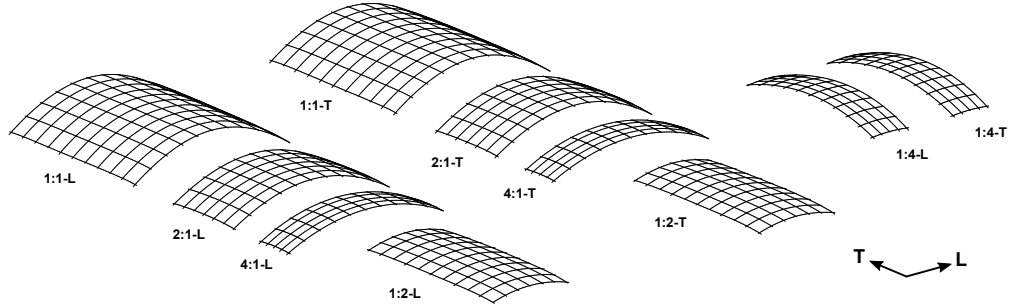


Figure 6. 3D scans of 4.9 mm thick and 1016 mm long 2024-T3 aluminum alloy rectangular sheets peened to full coverage at a 12×10^{-3} inches A Almen intensity with SCCW28 shot. All specimens, including 1:4 aspect ratio sheets, had their largest curvature along the L direction. The out of plane displacements were magnified by a factor of 4.

Table 6

Average curvatures of peened formed sheets and of the 254×254 mm coupons removed from the center of selected sheets.

Orientation [†]	Sheets: strokes parallel to L			Sheets: strokes parallel to T			Coupons		
	Specimen	Curvature ($\times 10^{-4}$ mm ⁻¹)		Specimen	Curvature ($\times 10^{-4}$ mm ⁻¹)		Removed from	Curvature ($\times 10^{-4}$ mm ⁻¹)	
		Along L	Along T		Along L	Along T		Along L	Along T
	Sheet 4:1-L	2.50	2.19	Sheet 4:1-T	2.46	2.07	Sheet 4:1-L	2.66	2.14
	Sheet 2:1-L	2.93	0.17	Sheet 2:1-T	3.06	0.11	Sheet 2:1-T	3.12	1.52
	Sheet 1:1-L	3.46	-0.01	Sheet 1:1-T	3.45	$\simeq 0$	Sheet 1:1-L	2.93	1.81
	Sheet 1:2-L	3.56	0.30 [‡]	Sheet 1:2-T	3.52	0.31 [‡]	Sheet 1:2-L	3.03	2.08
	Sheet 1:4-L	3.00	1.81	Sheet 1:4-T	2.93	1.94	Sheet 1:4-L	3.16	1.54

[†] Horizontal lines aligned with the L direction.

[‡] The curvature was approximately constant near the center and transitioned to 1.2×10^{-4} mm⁻¹ at approximately 200 mm from the edges.

ratio peened with 1.7 mm steel shot propelled at 53 m/s (a more intense peening treatment than that used here). Unlike in our experiments, however, Kulkarni's 2024-T3 aluminum specimens had their largest curvature along the T direction.

To give a sense of the shape of the sheets at intermediate stages of the peening process, Figure 7 shows the evolution of the deflection as a function of peening time for one sheet of each aspect ratio. These curves show that most of the forming occurred during the first 2 peening cycles, with diminishing returns for each additional cycle. After 12 cycles, most sheets had reached saturation, except for 1:1 and 2:1 aspect ratio specimens for which the positive slope suggests that additional peening could have resulted in larger deformations.

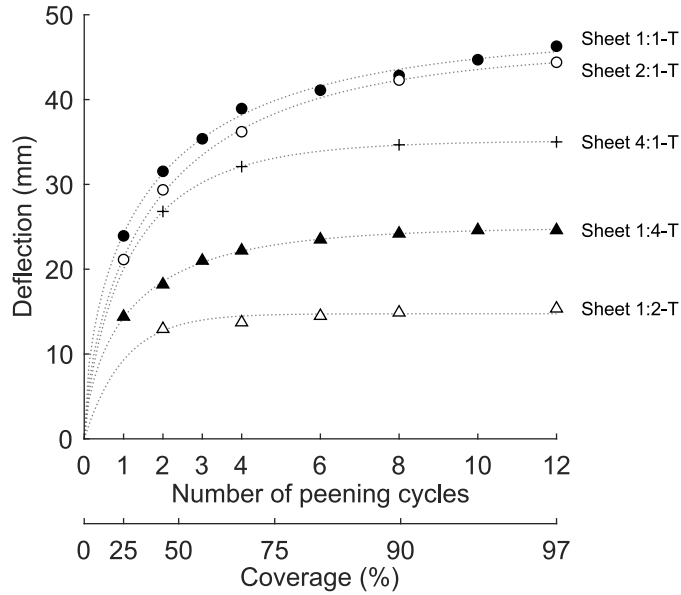


Figure 7. Deflection of specimens peened with strokes parallel to the T direction versus peening time. Similar curves were obtained for specimens peened with strokes parallel to the L direction. The dotted lines are a least-squares fit of $f(x) = a(1 - \exp(-bx^c))$, where a , b , and c are adjustable parameters.

235 Similar curves were obtained whether the sheets were peened with strokes parallel to the L or to the T direction.

240 Next, we consider the residual stresses inside the sheets. Figure 8 shows initial residual stresses measured by slitting in as-received material. Data were acquired over 70% of the thickness. Because both faces of a sheet experience the same sequence of operations during cold rolling, it is expected that initial residual stresses are symmetric. For this reason, the figure also shows as dotted lines a reconstruction of the entire residual stress profile obtained by mirroring data points with respect to the midplane of the specimen and by fitting smoothing splines through the cloud of points. The resulting profiles were almost in equilibrium; only a slight translation of 0.15 MPa towards positive stresses was needed to equilibrate axial loads. The shape of the profiles, with tensile stresses in the rolling direction and compressive stresses in the transverse direction, is typical of quenched and stress relieved heat treatable aluminum alloys (Dieter, 1961; Prime and Hill, 2002; Robinson et al., 2014).
 245 Figure 9 shows residual stresses measured by hole drilling in 254×254 mm

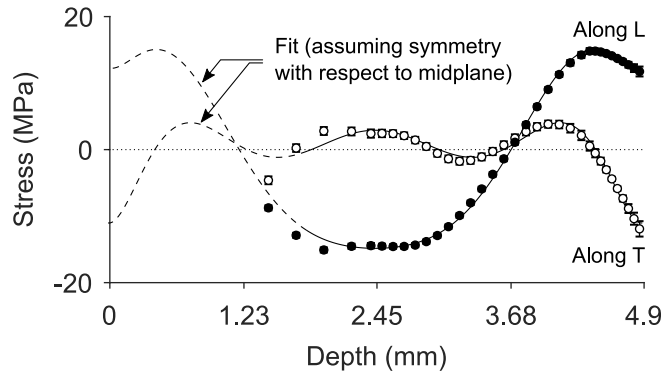


Figure 8. Residual stresses measured by the slitting method on two 51×51 mm coupons removed from an as-rolled sheet. Data were acquired up to a depth of 3.4 mm and through thickness profiles were reconstructed by assuming symmetry with respect to the midplane, fitting a smoothing spline through the cloud of points, and translating the resulting curve along the y axis to enforce forces equilibrium.

250 coupons removed from the center of the peened sheets. All profiles display maximum compressive residual stresses of approximately -380 MPa. The depth of the plastically deformed layer, that can be inferred from the location of the tensile residual stress peak (see Figure 1c), is about 0.5 mm in all cases. Note that, because of the stress relaxation that occurred when the coupons
 255 were removed from the sheets, residual stresses shown in Figure 9 differ from those that would have been measured in the as-peened sheets.

Finally, Figure 10a shows residual stresses in 15.24×17.78 mm coupons evaluated with the slitting method. This measurement was performed to cross-validate hole drilling measurements. In this case, profiles obtained with
 260 both methods are close except for the point closest to the surface, which provides the desired validation. Further investigating the differences between both sets of profiles would be hazardous as data were acquired on coupons of different geometries. Besides, hole drilling measurements are local while slitting tends to average stresses along the length of the slot and could be
 265 affected by edge effects due to the small size of the coupons.

Unlike hole drilling, which can only probe residual stresses in a shallow layer below the peened surface, slitting returns residual stress profiles much deeper into the material. From Figure 10a, it can be seen that, deeper than about 0.6 mm, residual stresses follow a linear trend, with some oscillations that
 270 are likely due to initial stresses resulting from the manufacturing process of

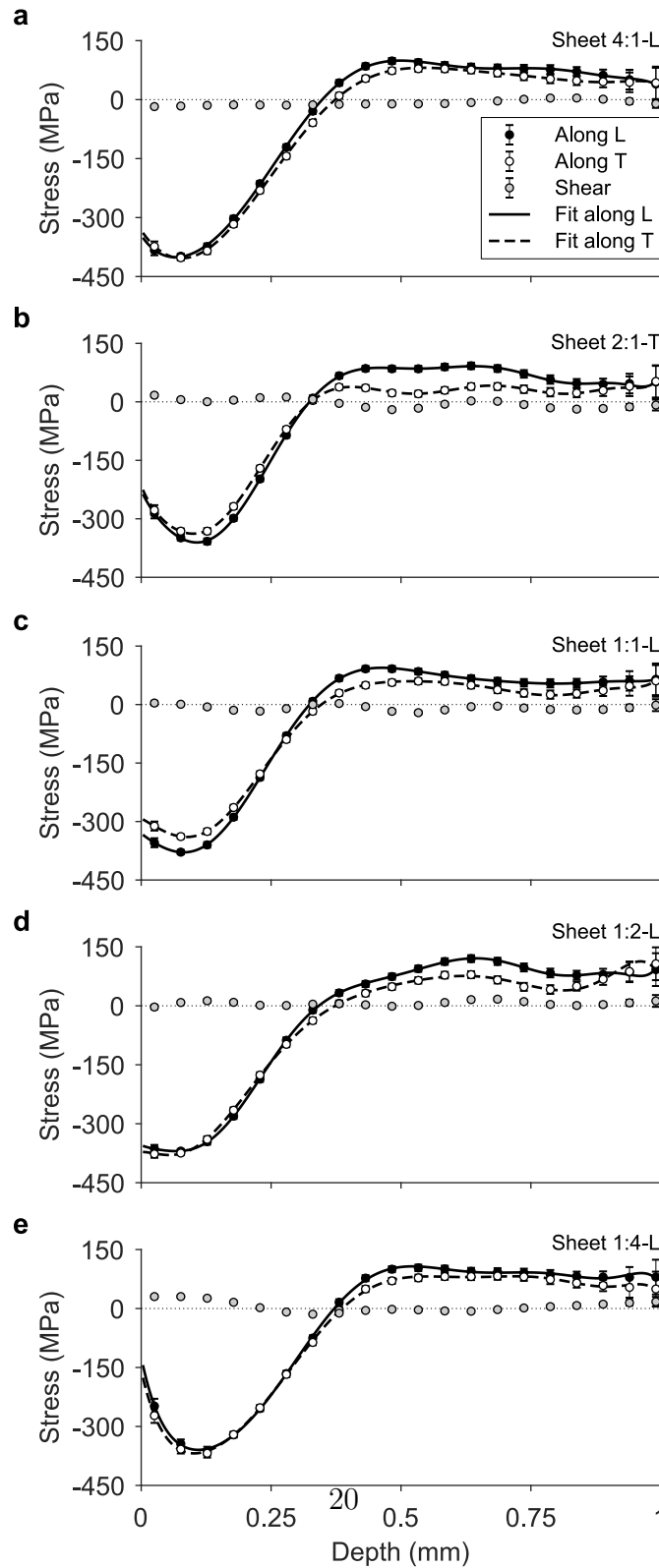


Figure 9. Residual stresses measured by hole drilling at the center of 254×254 mm coupons removed from the center of peen formed sheets. The fitting curves—shown only to guide the eye—are polynomial fits.

the sheets. This is confirmed in Figure 10b which shows the same data as in
in Figure 10a after subtraction of the linear part of the profile alongside the
initial stresses from Figure 8. Both sets of profiles have similar shape and
magnitude, which is consistent with our understanding of the process: since
275 peening only affects a thin layer of material near the surface, stresses below
the plastically deformed layer are equal to the initial stresses plus a linear
term due to stretching and bending of the specimens.

3.2. Stress peen forming experiments

Figure 11 shows the final unconstrained curvature of 508×127 mm strips
280 used for stress peen forming experiments as a function of prestress curvature.
The curvature along the prestress direction increases linearly with a slope of
approximately 0.23, regardless of the alignment of the strips with respect to
the rolling direction. The curvature along the transverse direction decreases
linearly with a slope of -0.03 for strips aligned with the L direction, and with
285 a slope of -0.13 for strips aligned with the T direction. The magnitude of
the slopes is consistent with results from the literature compiled in Table 1.
To the right of the dashed lines shown in Figure 11, which corresponds to
the curvature of identical unconstrained strips peened with the same treat-
ment, the final curvature is smaller than the prestress curvature (negative
290 springback), and vice versa.

Figure 12 shows residual stresses measured by hole drilling in 254×127 mm
coupons removed from the center of strips aligned with the L direction and
peened with increasing prestress curvatures. As prestress increases, near
surface stresses become more compressive. The largest variations occur along
295 the prestress direction, which causes the profiles to gradually separate. As
already noted by Barrett and Todd (1984), prestress appears to have little
effect on the depth of the plastically deformed layer. We also observe that,
whereas most profiles exhibit a local minimum approximately 0.1 mm below
the surface, residual stresses in the strip that was held flat during peening
300 do not. Whether this is due to prestress conditions or to variability in hole
drilling measurements cannot be assessed from the single profiles reported
here.

Figure 13 shows residual stresses measured under the same conditions in a
coupon removed from a strip that was free to deform during peening. The
305 shape of the profiles is similar to that for other coupons although stresses are
approximately 40 MPa higher (i.e., less compressive) over the first 0.2 mm.

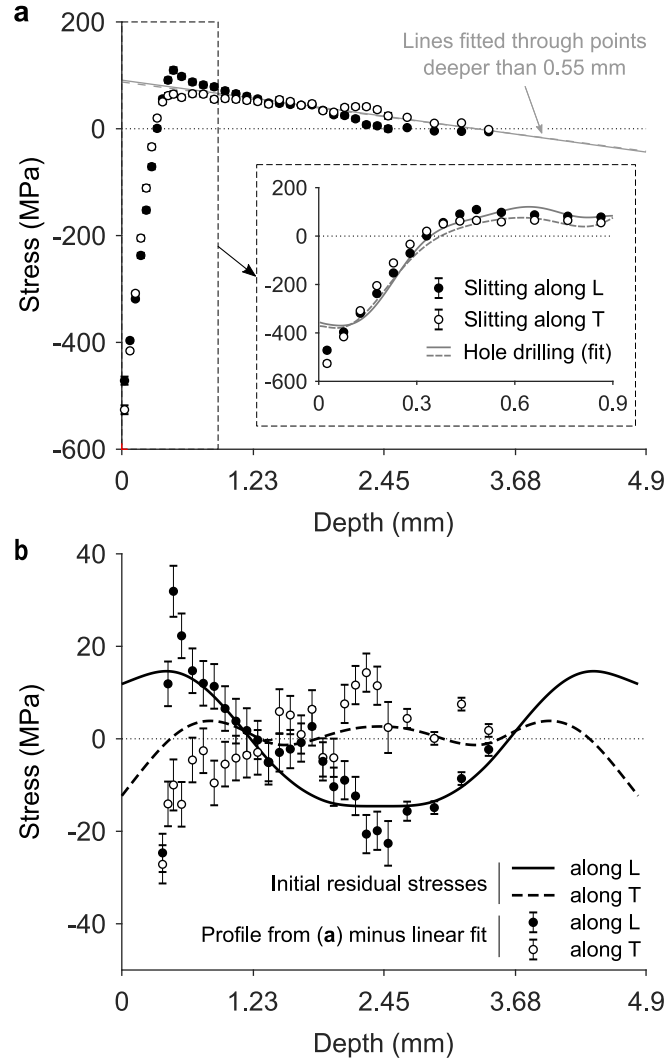


Figure 10. (a) Residual stresses measured by slitting in 17.78×15.24 mm coupons removed from sheet 1:2-L. Superimposed to the data is the fit to the residual stresses measured by hole drilling on the same sheet from Figure 9d. (b) Same data as in (a) after having subtracted the linear portion of the profile caused by bending and stretching of the specimens following peening. The latter was obtained by fitting a line through data points deeper than 0.55 mm. The oscillations thus isolated follow the same trend as that of the initial stresses shown in Figure 8.

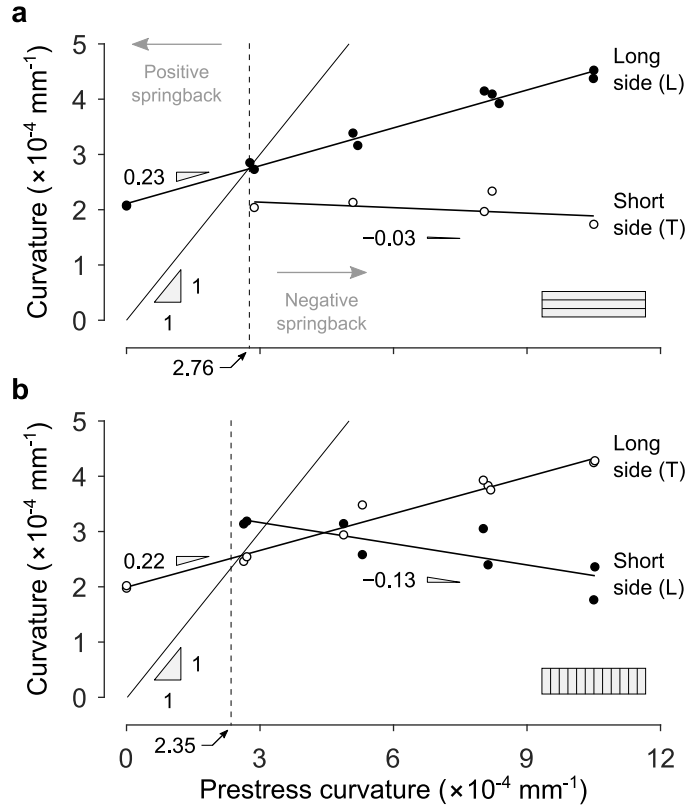


Figure 11. Average curvatures of 508×127 mm strips cut along (a) the L direction and (b) the T direction after all external constraints have been removed. All strips were peened with strokes parallel to their long side. Dashed lines show the curvature that unconstrained identical strips assumed when peened with the same treatment. Above this threshold, the curvatures of the strips are smaller than the prestress curvature (negative springback), and vice versa. Each point corresponds to one specimen. Eleven specimens were damaged before their curvatures along the short side could be measured.

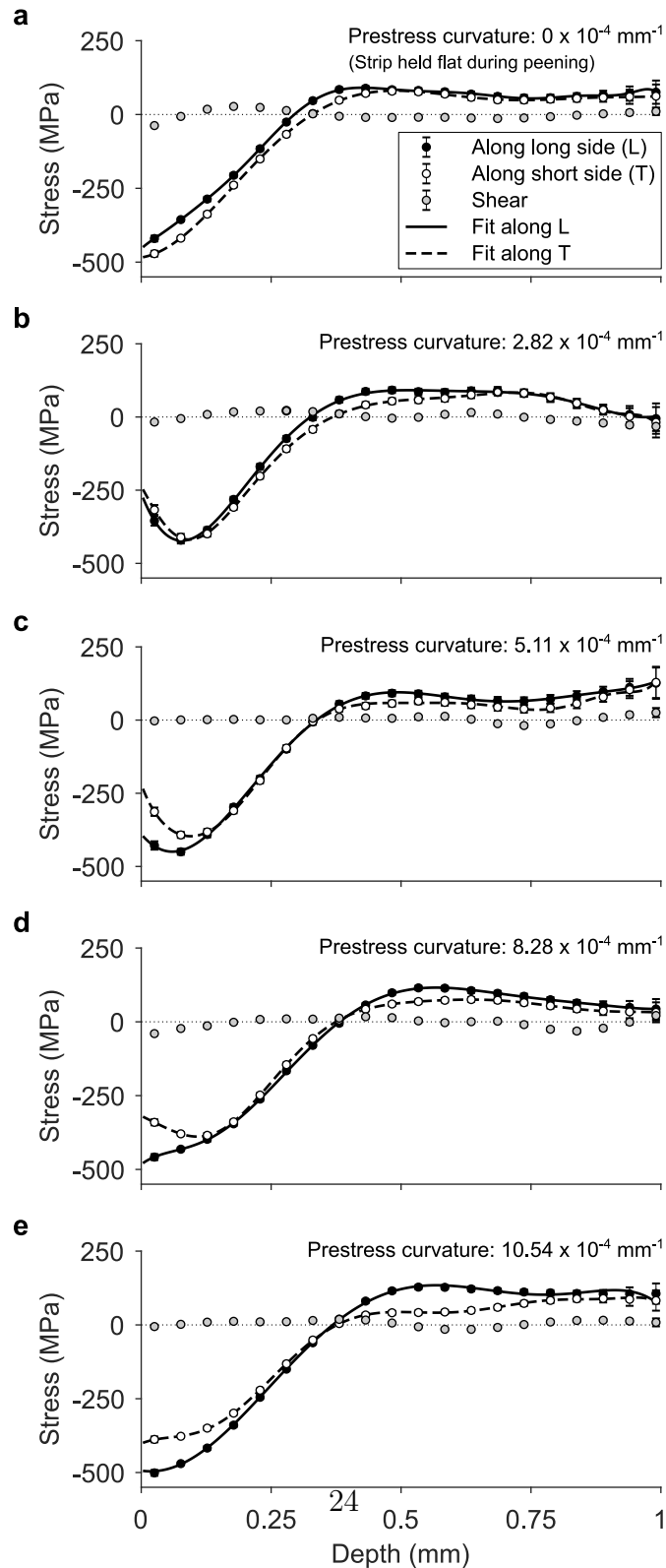


Figure 12. Residual stresses measured by hole drilling at the center of 254×127 mm coupons removed from the center of strips having their long side aligned with the L direction and peened with increasing prestress curvatures. The fitting curves—shown only to guide the eye—are polynomial fits.

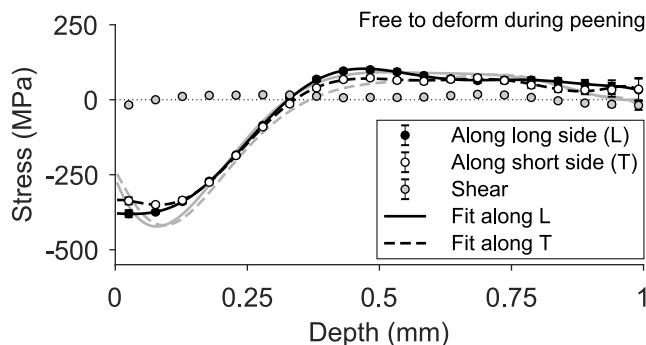


Figure 13. Residual stresses measured by hole drilling at the center of a 254×127 mm coupon removed from the center of a strip having its long side aligned with the L direction and that was free to deform during peening. The fitting curves—shown only to guide the eye—are polynomial fits. This strip assumed a curvature of $2.76 \times 10^{-4} \text{ mm}^{-1}$ along the long side. For comparison, the fit to residual stresses measured on the strip prestressed to $2.82 \times 10^{-4} \text{ mm}^{-1}$ from Figure 12b is shown as light grey curves.

Table 7

Curvature of strips that were held flat, prestressed to $2.7 \times 10^{-4} \text{ mm}^{-1}$ (nominal), and unconstrained during peening. All values $\times 10^{-4} \text{ mm}^{-1}$. Reported values were averaged over available results.

Long side aligned with	Held flat		Prestressed to $2.7 \times 10^{-4} \text{ mm}^{-1}$		Unconstrained	
	Along long side	Along short side	Along long side	Along short side	Along long side	Along short side
L	2.08	-	2.79	2.04	2.76	2.75
T	2.00	-	2.50	3.17	2.35	3.16

Table 7 compares the curvatures of 508×127 mm strips that were held flat during peening, prestressed to $2.7 \times 10^{-4} \text{ mm}^{-1}$, and unconstrained. Curvatures along the long side of unconstrained strips are reported as dashed lines in Figure 11. Unconstrained strips behave as if they had been prestressed into their final shape, peened, then released: except for curvatures along the short side of strips aligned with the L direction, the curvatures of unconstrained and prestressed strips differs by less than 6%. Their curvature is approximately 25% larger than that of strips that were held flat during peening.

4. Discussion

4.1. Preliminaries: natural curvatures

To interpret the results of peen forming experiments, a useful tool is the concept of natural curvature. Natural curvature is defined as the curvature of a small beam cut out from a plate at a given location and along a given direction (Pezzulla et al., 2016). It is natural in the sense that it is the curvature that the beam would spontaneously adopt if it were not constrained by surrounding material. The shape of a peen formed plate can therefore be seen as a compromise between the plate reaching its natural curvatures (locally) and satisfying the geometric constraints of plate mechanics (globally). In the case of shot peen parts, natural curvatures only depend on the thickness of the part and in the distribution of peening induced plastic strains.

Now, imagine that a small coupon is carefully removed from a larger shot peened plate and that removal does not alter the distribution of plastic strains in the coupon. If the deflection of the coupon is small compared to its thickness, then its curvatures are close approximations to the natural curvatures. Indeed, the response of a plate when deflections are small is linear and its stretching and bending modes are decoupled. Therefore, the coupon can attain its natural curvature in all directions without the bending in one direction affecting the bending in other directions, see (Timoshenko, 1940, section 23).

This is illustrated in Figure 14a for three geometries: that of strips used for stress peen forming experiments and that of the two types of coupons used for residual stress measurements. These curves were generated using the Abaqus finite element software by prescribing an equibiaxial thermal expansion ε^* in the upper half of a plate of thickness h and by ramping the expansion from zero. The natural curvature of this system is $3\varepsilon^*/2h$ (Timoshenko, 1925; van Rees et al., 2017). The plates were meshed with S4R elements and geometric nonlinearities were included in the analysis. For all three geometries, Figure 14a shows that simulated curvatures remain close to the natural curvature, even though a small deviation is observed for 254×254 mm coupons for natural curvatures larger than $2 \times 10^{-4} \text{ mm}^{-1}$. This deviation is due to nonlinear geometric effects: when out-of-plane deflections become of the same order as the thickness, stretching and bending mode are no longer decoupled and, since the spherical shape that the coupons adopt is non-developable, some of the elastic energy must contribute to stretching the coupons, which

reduces the amount available for bending, and results in a stiffening of the structure. Since the curvatures of prestressed strips (Figure 11) and the curvatures of coupons used for residual stress measurements (Table 6) are all smaller than $4 \times 10^{-4} \text{ mm}^{-1}$, we conclude from Figure 14a that these curvatures are close estimates of natural curvatures.

Note that, although the curves in Figure 14a were generated assuming equibiaxial expansion, the expansion in the peening affected layer of the actual specimens might not be. For example, plastic anisotropy or prestress might result in larger expansion in one direction. This, however, does not invalidate the fact that curvatures of small rectangular coupons are close approximations of natural curvatures when deflections are small.

4.2. Explaining the shape of large sheets

We now turn our attention to the shape of large sheets used for conventional peen forming experiments (Figure 6). Figure 14b shows curvatures as a function of natural curvature for the three geometries considered here. These curves were computed using the same finite element simulations as in section 4.1. In particular, we still used equibiaxial expansion as loads. Although the expansion in the actual specimens might not be equibiaxial, this simplified model still captures the main features of the response of uniformly peen formed plates.

In the linear domain, say for natural curvatures below $1 \times 10^{-5} \text{ mm}^{-1}$, all specimens deform into spherical shapes and their curvature is the same as the natural curvature. As natural curvature increases, the sheets remain spherical, but the curves depart from linearity due to stress stiffening. Because it is much easier to bend a thin plate than it is to stretch it, cylindrical shapes become energetically favorable for large natural curvatures (Pezzulla et al., 2016). For $1016 \times 1016 \text{ mm}$ plates, the transition occurs suddenly at approximately $0.86 \times 10^{-4} \text{ mm}^{-1}$, whereas curvatures along the long and short direction gradually diverge for the two other geometries.

Using the values in Table 6 as estimates for natural curvature, we found that the latter varied between 1.5 and $3.2 \times 10^{-4} \text{ mm}^{-1}$, depending on the specimen and on the direction. In this range, the curves in Figure 14b capture the main features of the experimentally observed deformed shapes: square plates deform into cylindrical shapes, 2:1 aspect ratio plates into elliptical shapes, and 4:1 aspect ratio plates into nearly cylindrical shapes.

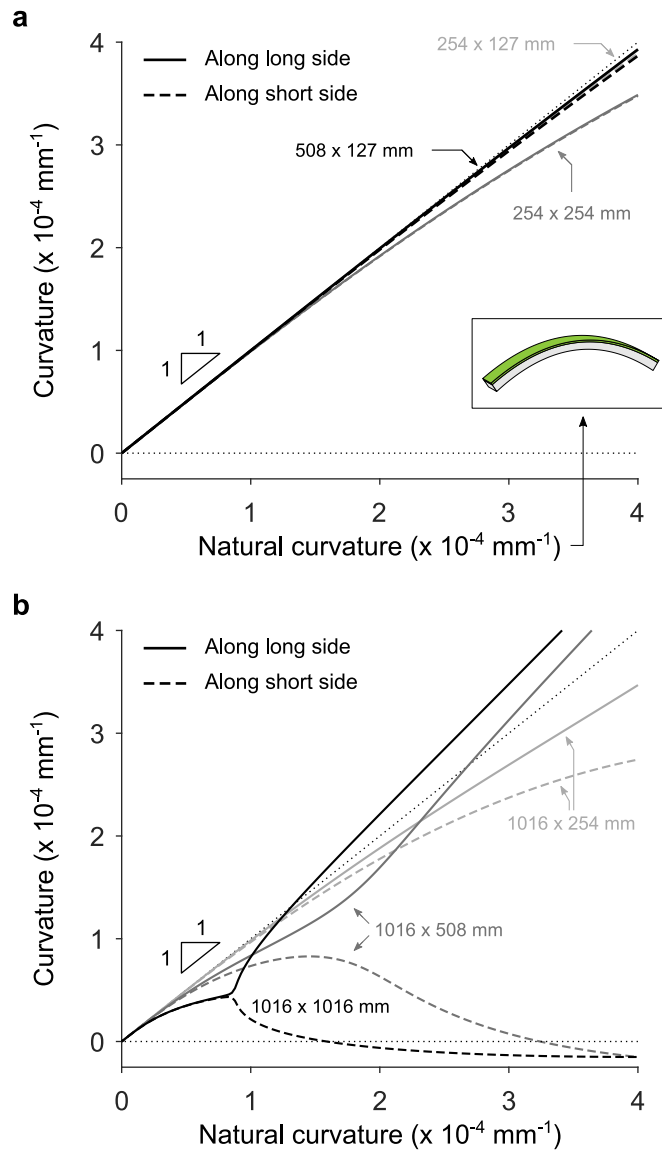


Figure 14. Curvature versus natural curvature for 4.9 mm thick rectangular plates of various dimensions. The curves were obtained from finite element simulations as described in Faucheux et al. (2018) assuming equibiaxial expansion in the peening affected layers. (a) For natural curvatures smaller than $3 \times 10^{-4} \text{ mm}^{-1}$, the relative difference between the identity line and the curves for 254 x 254 mm plates is less than 8.5%. It is less than 2% for 508 x 127 mm and 254 x 127 mm plates. Therefore, curvatures measured on such specimens are close estimates of natural curvatures. (b) Larger sheets exhibit more complex behaviors. In the linear domain, say for natural curvatures smaller than $1 \times 10^{-5} \text{ mm}^{-1}$, 1016 x 1016 mm, 1016 x 508 mm, and 1016 x 254 mm sheets deform into spherical shapes. As the natural curvature increases, geometric nonlinear effects become significant and the curves bend downward. When the natural curvature rises above $1 \times 10^{-4} \text{ mm}^{-1}$, 1016 x 1016 mm plates transition to cylindrical shapes due to an elastic instability. For all other geometries, no such transition occurs. Instead, curvatures along the long and short side gradually diverge.

From Figure 14b, we can also infer why specimens peened with strokes parallel to either the L or T direction deformed into identical shapes. For sheets of 1:1, 1:2, and 2:1 aspect ratio, this was likely because the sheets quickly
390 ‘locked’ into cylindrical shapes, which occurred during the first half of the first peening cycle. Once in this configuration, a sheet can only continue bending in the same direction as its geometric rigidity resists other deformation modes. The precise peening trajectory is then of little importance if the specimens are peened until their deformation saturates, as was the case here
395 (Figure 7). The same reasoning applies to 1:4 and 4:1 aspect ratio specimens which, although they do not ‘lock’, can only deform into nearly spherical shapes.

4.3. Influence of material anisotropy

Simulations in Figure 14 predict that, when the expansion in the peening
400 affected layers is equibiaxial, rectangular sheets spontaneously bend along the long side. This phenomenon was explained by Alben et al. (2011) which showed that highly localized regions of double curvature along the free edges of bilayer systems reduce the elastic energy of the system and make long side bending energetically favorable.

405 However, not all our specimens bent along the long side. Instead, all had their largest curvature along the L direction, even when the L direction was aligned with the short side. This is especially clear for 2:1 and 1:2 aspect ratio sheets which—for otherwise identical peening conditions—deformed into cylinders if their long side was aligned with L, and into flatter elliptical shapes
410 if their long side was aligned with T (Figure 6). Because the only difference between these two sets of sheets was their alignment with the rolling direction, these results suggest that some form of material anisotropy resulted in larger expansion in the L direction, with the level of anisotropy being sufficiently strong to overcome the geometrical preference for the sheets to bend
415 along their short side.

Although the 2024–T3 aluminum sheets used here had isotropic elastic properties, tensile tests revealed a mild plastic anisotropy (Table 3). Therefore, we expect that more plastic flow would occur along some direction after each impact, resulting in larger plastic strains, hence curvatures, along this direc-
420 tion. However, it is not clear from the limited tensile test results available that this direction is the L one. Checking that this is the case would require compression or indentation tests.

Another possible source of material anisotropy is the initial residual stresses. Their effect can be explained as follows. In as-received sheets, residual stresses are symmetric with respect to the midplane of the sheets (Figure 8) and, therefore, do not induce curvature. This symmetry, however, is broken when peening induces large compressive residual stresses near the surface. When compared to an initially stress-free specimen, residual stresses on the back face amplify or reduce the amount of curvature that the specimen experiences, depending on their sign. Quantifying the contribution of this effect is deferred to Part 2 of this paper [Miao et al. \(2021\)](#).

4.4. Influence of prestress

Another source of anisotropy is prestress. Here, we extend the use of the term ‘prestress’ to designate both externally applied loads (as in stress peen forming experiments) and internal loads (as in conventional peen forming experiments) that cause a sheet to assume a compound curvature. Initial stresses before an impact depend on the direction of the prestress and cause larger plastic strains to develop in the direction in which stresses are the largest (i.e., the more tensile, or the less compressive).

This effect is most clearly seen in the curvature of strips used for stress peen forming tests which is always larger along the prestress direction (Figure 11). It also affects the shape of unconstrained sheets that were free to deform during peening as evidenced by the fact that coupons removed from specimens used for conventional peen forming tests all had different curvatures. Indeed, recall that the curvatures of the coupons are close estimates of natural curvature, and that the latter only depends on the thickness of the coupon and on the distribution of plastic strains. Had the progressive deformation of the specimen had no effect, all coupons would have assumed the same curvatures since they were removed from specimens made from the same material and peened in the same conditions.

This effect is also apparent in Figure 7 which shows that the deflection of sheets of different geometries saturated after different numbers of peening cycles. For example, sheet 1:2-T saturated after approximately five cycles whereas sheets 1:1-T and 2:1-T had not reached saturation after twelve cycles. Had the progressive deformation of the specimen had no effect, all curves would have saturated at the same time.

Finally, notice how residual stresses measured in coupons removed from

460 sheets 2:1-T and 1:1-L, which deformed into cylindrical shapes, exhibited larger compressive stresses along the bending direction (Figure 9b-c) whereas residual stresses in coupons removed from other sheets, which deformed into elliptical or nearly spherical shapes, were almost equibiaxial (Figure 9a, d, e).

5. Conclusion

465 In this paper, we presented the results of conventional and stress peen forming experiments conducted on 4.9 mm thick 2024-T3 aluminum sheets shot peened to full coverage with the same low intensity treatment. Our results highlight features of the response of thin peen formed sheets that were known to process engineers but that had been poorly documented so far. In particular, we illustrated why squares are susceptible to elastic instabilities but elongated strips less so, and we showed that the final shape of a peen formed sheet 470 does depend on the way the sheet deforms during peening—this deformation having the same effect as an externally applied prestress. We also observed a preferential bending of all specimens along the L directions and discussed why this behavior must be a manifestation of material anisotropy—in the form of plastic anisotropy or non-equibiaxial initial stresses inherited from 475 earlier processing stages (e.g., heat treatment, rolling).

The other main observations are as follows.

1. Identical specimens peened until their deformation saturated assumed identical shapes, regardless of the peening trajectory.
- 480 2. The curvatures of prestressed strips varied linearly with the prestress curvature.
3. There exists a critical prestress curvature such that, when constraints are removed, a prestressed strip does not spring back. This curvature coincides with that which the strip would assume if it was free to deform 485 during peening.
4. If a strip is prestressed to a smaller curvature than this critical value (for example, if it is held flat during peening), it will bend less than if it is free to deform, and vice versa.

490 Although similar behaviors were observed in earlier works, residual stress measurements along both directions before and after peening were seldom

reported. This information is needed to understand how different sources of anisotropy—such as prestress, plastic anisotropy, and non-equibiaxial initial stresses—affect the final deformed shapes. Furthermore, such measurements enable to identify peening-induced plastic strains which provide much clearer insights into the mechanics of peen formed plates than residual stresses alone, as will be demonstrated in Part 2 of this paper [Miao et al. \(2021\)](#).

6. Acknowledgements

The authors gratefully acknowledge financial support from Airbus, from the Rio Tinto group through a graduate scholarship, from the Canada Research Chairs program, and from the Natural Sciences and Engineering Research Council of Canada (NSERC; funding reference number 175791953). The prestressing jig used for stress peen forming experiments was courtesy of Aérospère and Centre Technologique en Aérospatiale (CTA).

References

- D. L. Baughman, Peen forming, *Machine design* 42 (1970) 156–160.
- A. Levers, Broughton: From Wellington bombers to the A380, *The International Journal for the History of Engineering & Technology* 80 (2010) 55–79.
- K. Hornauer, W. Köhler, Development of the peen forming process for spherical shaped components, in: *Proceedings of the 4th International Conference on Shot Peening (ICSP4)*, Tokyo, Japan, 1990, pp. 585–594.
- J. Merino, A. Patzelt, A. Steinacher, M. Windisch, G. Heinrich, R. Forster, C. Bauer, *Ariane 6 - Tanks & structures for the new european launcher*, München, 2017, p. 10.
- R. D. Skinner, Stress-peen straightening of complex machined aircraft parts, in: *Formability Topics—Metallic Materials*, ASTM International, 1978, pp. 100–121.
- J. Eckersley, D. Axline, B-727 brake components salvaged by shot peen forming, in: *Proceedings of the 27th annual aerospace/airline plating and metal finishing forum*, San Antonio, Texas, US, 1991.

- A. Gariépy, Finite element modelling of shot peening and peen forming processes and characterisation of peened AA2024-T351 aluminium alloy, Ph.D. thesis, École Polytechnique de Montréal, 2012.
- 525 K. M. Kulkarni, J. A. Schey, D. V. Badger, Investigation of shot peening as a forming process for aircraft wing skins, *Journal of Applied Metalworking* 1 (1981) 34–44.
- A. P. Villalva-Braga, Análise de ligas de alumínio aeronáuticas conformadas por jateamento com granalhas-caracterização e previsão de deformação, Master’s thesis, Universidade de São Paulo, 2011.
- 530 H. Y. Miao, D. Demers, S. Larose, C. Perron, M. Lévesque, Experimental study of shot peening and stress peen forming, *Journal of Materials Processing Technology* 210 (2010) 2089–2102.
- M. B. Prime, Amplified effect of mild plastic anisotropy on residual stress and strain anisotropy, *International Journal of Solids and Structures* 118-119 (2017) 70–77.
- 535 (2017) 70–77.
- A. Gariépy, S. Larose, C. Perron, P. Bocher, M. Lévesque, On the effect of the orientation of sheet rolling direction in shot peen forming, *Journal of Materials Processing Technology* 213 (2013) 926–938.
- P. A. Faucheux, F. P. Gosselin, M. Lévesque, Simulating shot peen forming with eigenstrains, *Journal of Materials Processing Technology* 254 (2018) 135–144.
- 540 (2018) 135–144.
- C. F. Barrett, R. Todd, Investigation of the effects of elastic pre-stressing technique on magnitude of compressive residual stress induced by shot peen forming in thick aluminum plates, in: *Proceedings of the Second International Conference on Shot Peening*, Chicago, 1984, pp. 15–21.
- 545 (1984) 15–21.
- Y. Hu, Z. Li, X. Yu, Z. Yao, Effect of elastic prestress on the laser peen forming of aluminum alloy 2024-T351: Experiments and eigenstrain-based modeling, *Journal of Materials Processing Technology* 221 (2015) 214–224.
- K. Li, Using stress peen-forming process for integrally stiffened wing panels, in: *Proceedings of the First International Conference on Shot Peening*, Paris, France, 1981, pp. 555–563.
- 550 (1981) 555–563.

- H. Miao, S. Larose, C. Perron, M. Lévesque, Numerical simulation of the stress peen forming process and experimental validation, *Advances in Engineering Software* 42 (2011) 963–975.
- 555 M. T. Wang, Y. S. Zeng, X. P. Bai, X. Huang, Deformation rule of 7150 aluminum alloy thick plate by pre-stress shot peen forming, *Advanced Materials Research* 1052 (2014) 477–481.
- X. Xiao, Y. Wang, W. Zhang, J. Wang, S. Wei, Numerical research on stress peen forming with prestressed regular model, *Journal of Materials Processing Technology* 229 (2016) 501–513.
- 560 T. Zhang, L. Li, S.-h. Lu, J.-b. Zhang, Z. Zhou, H. Gong, Effect of prestressed ultrasonic peen forming parameters on bending curvature and spherical deformation of plate, *Transactions of Nonferrous Metals Society of China* 29 (2019) 270–278.
- 565 SAE standard J2277, Shot Peening Coverage Determination, Standard, SAE International, 2013.
- SAE standard J443, Procedures for Using Standard Shot Peening Almen Strip, Standard, SAE International, 2010.
- W. Cao, R. Fathallah, L. Castex, Correlation of Almen arc height with residual stresses in shot peening process, *Materials science and Technology* 11 (1995) 967–973.
- 570 B. Cina, T. Kaatz, I. Eldror, The effect of heating shot peened sheets and thin plates of aluminium alloys, *Journal of materials science* 25 (1990) 4101–4105.
- 575 M. Gelineau, Étude de l’impact du grenailage sur des composants mécaniques industriels à géométrie complexe, Ph.D. thesis, École Nationale Supérieure d’Arts et Métiers, 2018.
- W. Johnson, A. G. Mamalis, S. K. Ghosh, On the peen-forming of metals, in: *Proceedings of the Twenty-First International Machine Tool Design and Research Conference*, Palgrave, London, 1981, pp. 85–93.
- 580 A. Gariépy, S. Larose, C. Perron, M. Lévesque, Shot peening and peen forming finite element modelling – Towards a quantitative method, *International Journal of Solids and Structures* 48 (2011) 2859–2877.

- ASTM standard B557M-15, Standard test methods for tension testing
585 wrought and cast aluminum- and magnesium-alloy products (metric),
Standard, ASTM International, West Conshohocken, PA, 2015.
- F. Bron, J. Besson, A yield function for anisotropic materials. Application
to aluminum alloys, *International Journal of Plasticity* 20 (2004) 937–963.
- J. Seidt, A. Gilat, Plastic deformation of 2024-T351 aluminum plate over
590 a wide range of loading conditions, *International Journal of Solids and
Structures* 50 (2013) 1781–1790.
- AMS standard 2431/8B, Peening Media (AWCH) Conditioned Carbon Steel
Cut Wire Shot, High Hardness (55 to 62 HRC), Standard, SAE Interna-
tional, 2007.
- 595 AMS standard 2430 rev. T, Shot Peening, Automatic, Standard, SAE Inter-
national, 2015.
- M. B. Prime, Residual stress measurement by successive extension of a slot:
The crack compliance method, *Applied Mechanics Reviews* 52 (1999) 75–
96.
- 600 G. S. Schajer, M. B. Prime, Use of inverse solutions for residual stress mea-
surements, *Journal of Engineering Materials and Technology* 128 (2006)
375.
- M. B. Prime, M. R. Hill, Uncertainty, model error, and order selection for
series-expanded, residual-stress inverse solutions, *Journal of Engineering*
605 *Materials and Technology* 128 (2006) 175–185.
- ASTM standard E837-08, Standard Test Method for Determining Residual
Stresses by the Hole-Drilling Strain-Gage Method, Standard, ASTM In-
ternational, West Conshohocken, PA, 2008.
- G. E. Dieter, Mechanical metallurgy, *Metallurgy and Metallurgical Engineer-
ing Series*, McGraw-Hill, New York, 1961.
610
- M. B. Prime, M. R. Hill, Residual stress, stress relief, and inhomogeneity in
aluminum plate, *Scripta Materialia* 46 (2002) 77–82.

- 615 J. S. Robinson, D. A. Tanner, C. E. Truman, The origin and management of residual stress in heat-treatable aluminium alloys: Origin and management of residual stresses, *Strain* 50 (2014) 185–207.
- M. Pezzulla, G. P. Smith, P. Nardinocchi, D. P. Holmes, Geometry and mechanics of thin growing bilayers, *Soft Matter* 12 (2016) 4435–4442.
- S. Timoshenko, *Strength of materials; Part II; Advanced theory and problems*, 2nd ed. ed., D. Van Nostrand Company, Inc., 1940.
- 620 S. Timoshenko, Analysis of bi-metal thermostats, *Journal of the Optical Society of America* 11 (1925) 233–255.
- W. M. van Rees, E. Vouga, L. Mahadevan, Growth patterns for shape-shifting elastic bilayers, *Proceedings of the National Academy of Sciences* 114 (2017) 11597–11602.
- 625 S. Alben, B. Balakrishnan, E. Smela, Edge effects determine the direction of bilayer bending, *Nano Letters* 11 (2011) 2280–2285.
- H. Y. Miao, M. Levesque, F. P. Gosselin, Peen forming and stress peen forming of 2024-t3 aluminum sheets. Part 2: eigenstrain analysis (2021). Manuscript submitted for publication to *Strain*.